Kinetic Modeling of the Photocatalytic Degradation of Air-Borne Pollutants

H. Ibrahim and H. de Lasa
Chemical Reactor Engineering Center, Faculty of Engineering Science, The University of Western Ontario, London, Ontario N6A 5B9, Canada

DOI 10.1002/aic.10097
Published online in Wiley InterScience (www.interscience.wiley.com).

The photocatalytic conversion of organic model pollutants (acetone, acetaldehyde, and isopropanol) in a novel Photo-CREC-Air unit is considered. This photocatalytic unit features: (1) external near-UV lamps placed in parabolic reflectors, (2) a basket supporting the irradiated glass mesh holding TiO_2 loadings to achieve high photoconversion rates, and (3) a fluid flow pattern securing high gas velocities in the near-mesh region. Given the high quantum efficiencies observed in Photo-CREC-Air and, as a result, the high prospects for this novel design, rate equations and associated mechanistic formulations are investigated. With this goal, a Langmuir–Hinshelwood model, involving a one-site model pollutant mechanism, is considered. The associated kinetic parameters with the related statistical indicators are established, using least-square nonlinear regression. It is found that this model is adequate for describing the photodegradation of acetone on both Degussa P25 and Hombikat UV-100. It is also observed that the same type of reaction rate model is less adequate for the photodegradation of acetaldehyde and isopropanol, in particular, for predicting the formation of carbon dioxide. © 2004 American Institute of Chemical Engineers *AIChE J,* 50: 1017–1024, 2004
Keywords: photodegradation, photocatalysis, kinetic modeling, air-borne pollutants, Langmuir–Hinshelwood model

Introduction

Heterogeneous photocatalytic oxidation of organic contaminants in air streams is a promising technology because of some distinctive advantages, including the potential for lower operating costs (Miller and Fox, 1993); the elimination of treatment reagents or electron acceptors, such as H_2O_2 (Miller and Fox, 1993; Suri et al., 1993); the possible recovery, regeneration, and reuse of the photocatalyst (Suri et al., 1993); and the applicability to a wide spectrum of organic compounds for complete mineralization (Suri et al., 1993). Cabrera et al. (1994) indicated that almost any organic and many of the inorganic pollutants, produced by the various industries, can be completely mineralized by heterogeneous photocatalysis.

Correspondence concerning this article should be addressed to H. de Lasa at hdelasa@eng.uwo.ca.

In addition, the photocatalytic technology can be used in conjunction with solar radiation (Suri et al., 1993), at close to ambient temperature (Cassano et al., 1995; Falconer and Magrini-Bair, 1998; Miller and Fox, 1993). Photocatalysis also shows important prospects for certain air treatment applications, given the observed apparent quantum efficiencies exceeding the 100% level (Ibrahim and de Lasa, 2003).

Heterogeneous photocatalysis steps were reviewed between others by Yue (1993), Jacoby et al. (1996), and Cunningham and Hodnett (1981). This includes the mass transfer of substrate from the bulk fluid to the catalyst surface, the transport of the reactants within the catalyst particle, and the adsorption of substrates on the active catalytic surface. Moreover, once the TiO_2 is irradiated, there is absorption of the photon energy, followed by the generation of electron-hole pairs, the formation of radicals, the surface reaction, the radical recombination, and finally the desorption and mass transfer of products out of the particle surface and into the bulk of the fluid.

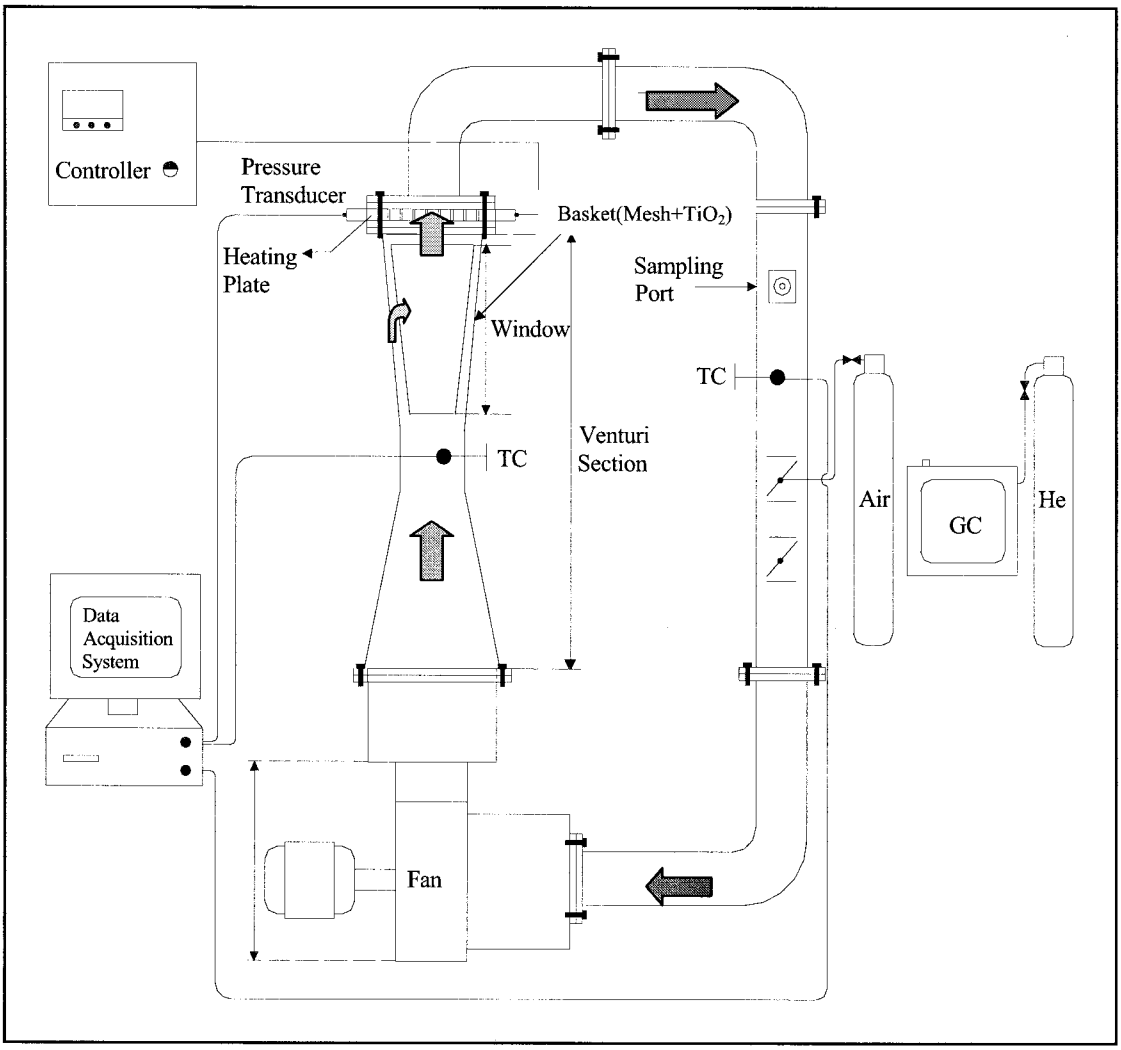

Figure 1. Photo-CREC-Air unit setup.

Additional details are given in Ibrahim (2001).

Under certain conditions, however, some of these steps may not need to be considered. For instance, if the photocatalyst particle is not porous, the mass transfer process within the catalyst particle can be ignored. In addition, in reactors where there is a high fluid velocity contacting the catalyst, mass transport limitations on the surface of the TiO_2 particles may be neglected, with the intrinsic photocatalytic reaction becoming the controlling step (Jacoby et al., 1996).

Mathematical models have been developed to describe the behavior of the oxidation of organic compounds over titanium dioxide. Postulated models include: (1) Langmuir–Hinshelwood models involving the reaction between adsorbed oxygen and adsorbed reactant molecules (Luo and Ollis, 1996; Nimlos et al., 1996; Peral and Ollis, 1992), and (2) Eley–Rideal models considering the reaction between adsorbed oxygen and gas phase reactant molecules (Fox, 1988). In this respect, Cunningham and Hodnett (1981) suggested a combination of Langmuir–Hinshelwood and Eley–Rideal kinetics.

The novel Photo-CREC-Air reactor, of the present study, optimizes irradiation of the mesh as well as the contacting of the air with the supported TiO_2. This novel configuration highlights TiO_2 supported on fiberglass mesh and a Venturi section displays high catalytic performance with high apparent quantum efficiencies, greater than 100% (Ibrahim and de Lasa, 2003). It is under these conditions of high reactor performance that kinetic modeling of the photodegradation of organic model compounds, as attempted in this study, becomes especially relevant.

Experimental Setup and Methods

Experimental studies of the photocatalytic conversion of air pollutants were carried out in a laboratory-scale version of Photo-CREC-Air (Figure 1) using immobilized nonporous 35–36 m^2/g Degussa P25 particles and porous 300 m^2/g Hombikat UV-100 particles (Ibrahim and de Lasa, 2002).

The main body of the 14.7-L capacity closed-loop system is made of straight zinc-plated pipes connected with aluminized-steel 90° elbows and a stainless steel Venturi section. External lamps irradiate the reaction section. Radiation evolves through windows cut out of acrylic sheets (UL Light Technology, Birmingham, U.K.) placed in the divergent section of the Venturi. Eight Pen-Ray 1-watt lamps were symmetrically

placed around the reaction section and housed in reflectors for uniform irradiation of the reacting section (Ibrahim, 2001). The reaction section is constituted by a basket supporting fiberglass mesh and immobilized TiO_2. Additional details about the TiO_2 mesh used as well as the various impregnation techniques adopted are reported in Ibrahim and de Lasa (2002).

The lamp intensity spectrum was measured using the SolaScope 2000 spectroradiometer for the 300–390 nm range for every 0.5 nm. Ibrahim (2001) showed that measurements performed with the SolaScope 2000 probe at different locations of the Photo-CREC-Air unit confirmed the uniform intensity distribution of photons provided by external lamps and reaching the 510 m^2 glass fiber mesh area holding the optimum loadings of TiO_2: 8.0–8.8 wt. % for Degussa P25 and 3.6–4.8% for Hombikat UV-100 (Ibrahim and de Lasa, 2002). Radiation exiting the Pen-Ray lamps was estimated at 0.068 watts, whereas radiation reaching the mesh was assessed at 0.02 watts, providing an overall efficiency of 29.4%.

Development of the Photo-CREC-Air reactor was accomplished, in this study, through the characterization of fluid flow patterns in the unit and through the assessment of the UV radiation reaching the impregnated mesh. Regarding calculation of the fluid flow patterns and the fluid flow visualization, they were developed using CFX-4.3 software for fluid flow simulation. In simulating the flow patterns, in the Venturi section, it was assumed as having a plane of symmetry in both the x and y directions. This allowed subdividing its physical volume into four quarters. This was done to be able to use smaller cell sizes and to improve convergence (Ibrahim, 2001).

Results from the simulated flow show that the proposed design provides the highest gas velocity in the near window region, securing a high degree of window sweeping and preventing TiO_2 particle deposition on the acrylic windows. Also the proposed design ensures in the near-mesh region a uniform velocity distribution (10–15 m/s), which secures good contact between the fluid containing the pollutants and the TiO_2 particles held on the mesh.

Photo-CREC-Air unit operates in a batch mode with a given amount of model pollutant injected in a set volume of air. Model pollutants were, in the present study, vaporized almost instantaneously and mixed intimately with the air stream. After the completion of adsorption, which typically lasted between 20 min to 1 h, with acetaldehyde requiring shorter times than acetone and isopropanol, the lamps were turned on and the changes in the chemical species concentrations with reaction time were studied. The process of photoconversion continued until the gas-phase pollutant concentrations reached low enough levels of detection. Photodegradation of pollutants and removal efficiency were in all cases above 90%.

Given that the available oxygen in air was well in excess with respect to that required from the combustion stoichiometry, experiments were developed with organic model pollutant as the limiting reagent. As a result oxygen effects were neglected in the kinetic modeling.

Three model pollutants were used during this study. They included isopropanol, acetone, and acetaldehyde (all supplied by Caledon Laboratories Ltd.) with at least 99% purity. For acetone and isopropanol injections of 40, 50, and 60 μL of the liquid pollutant into the 14.7-L reactor volume were used, to attain the desired gas phase concentrations. On the other hand, in the case of acetaldehyde 30, 40, and 50 μL of liquid were used to reach the desired initial pollutant concentrations. A gas chromatograph HP 5890 equipped with an HP3393A integrator, a TCD, and a Poropak Q packed column allowed the identification and quantification of chemical species, and this included product intermediates and carbon dioxide.

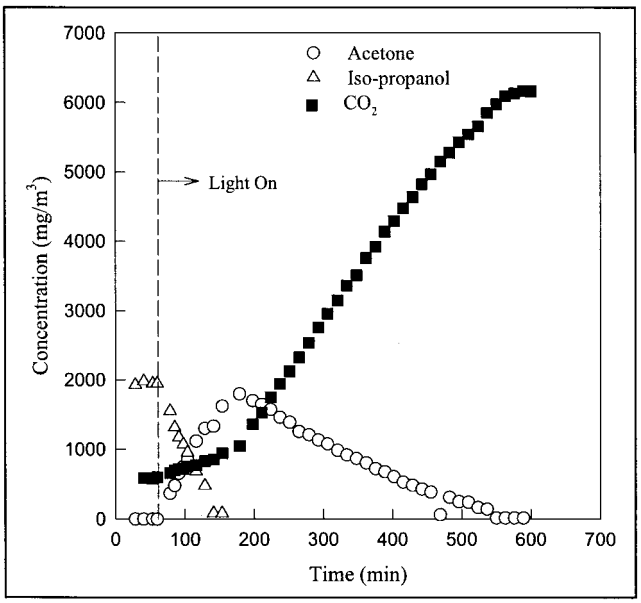

Figure 2. Photoconversion of isopropanol using Hombikat UV-100.

Gas-phase chemical species concentration changes with reaction time using Hombikat UV-100.

Additional details of the Photo-CREC-Air unit, experimental procedures, and the analytical techniques used are reported in Ibrahim and de Lasa (2002) and Ibrahim (2001).

Experimental Results

Blank experiments are needed to show that the photoconversion reaction did not proceed without the presence of either the TiO_2 or the UV radiation, to discount the potential influence of the reaction on equipment materials. Blank runs were conducted using isopropanol, acetone, and acetaldehyde as model pollutants (Ibrahim, 2001). Results obtained showed that under "dark reaction" conditions (no UV radiation) there was negligible conversion of the model pollutants. A similar behavior was observed when lamps were turned on with TiO_2 mesh being removed from the unit. Thus, it is shown, in agreement with Suzuki (1993) and Shifu et al. (1998), that the photoconversion reactions require the presence of both TiO_2 and UV radiation.

For isopropanol no stable by-products, besides acetone, were detected in the gas phase. It was noticed that the isopropanol concentration decreases continuously with reaction time, whereas the acetone concentration increases, first reaching a maximum, and then decreases. Regarding carbon dioxide concentration, it increases consistently with reaction time. Experiments with isopropanol (Figure 2) consistently showed that the photocatalytic oxidation of isopropanol proceeds, at room temperature, by a zero-order reaction, whereas the photocatalytic conversion of acetone (Figure 3) was a first-order reaction. On the basis of these data one can argue that the isopropanol

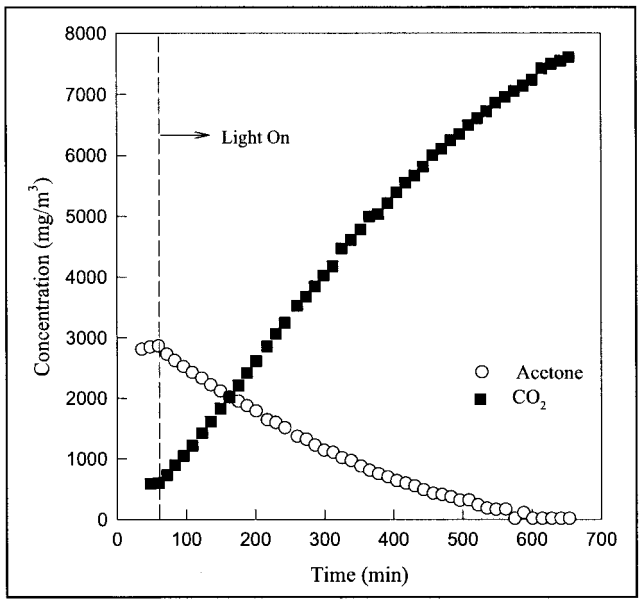

Figure 3. Photoconversion of acetone using Hombikat UV-100.

Gas-phase chemical species concentration changes with reaction time.

conversion involves two steps overall in series, with the first step involving a fast transformation of isopropanol into acetone, which is followed by a slower acetone oxidation step into carbon dioxide and water. On this basis, it can be speculated that both isopropanol and water compete for the same TiO_2 sites, with isopropanol having a stronger adsorption affinity.

Experiments with acetone (Figure 3), as the primary model pollutant, showed that acetone photodegradation rate is much slower than that of isopropanol. Results showed that almost complete conversion of acetone was achieved with no by-products, other than those of complete combustion. In this respect, acetone photocatalytic oxidation results are in agreement with those of Peral and Ollis (1992) and Raupp and Junio (1993).

Concerning acetaldehyde, the photoconversion reaction (Figure 4) was observed to be much faster than that for acetone. Acetaldehyde was completely converted, showing no gas-phase intermediate products. However, acetic acid was detected on the catalytic mesh surface extract under conditions of incomplete model pollutant conversion. Given that no acetic acid was observed in the gas phase, it was speculated that acetic acid had a strong adsorption affinity with the TiO_2-mesh system, thus preventing its gas phase detection. Ohko et al. (1998) reported similar findings, with a catalyst extract revealing the presence of acetic acid. This unaccounted acetic acid is, after Ohko et al. (1998), necessary to close the carbon balance. In this respect, the acetic acid adsorption constant reported by Nimlos et al. (1996) was quoted as being three and 14 times larger than that for ethanol and for acetaldehyde, respectively.

Photoreaction modeling

To establish a kinetic model on the basis of experiments developed in the Photo-CREC-Air unit, a number of assumptions regarding the operation of this unit should apply (Ibrahim, 2001):

(1) Uniform gas airflow across the mesh, providing both intimate contact of the air flow with the supported TiO_2 and essentially constant species gas phase concentrations throughout the unit at any given reaction time. This is achieved as a result of adequate pressure drop across the mesh and the high air gas recirculation in a reactor operating under batch conditions.

(2) Uniformly and constant irradiation of the mesh supporting the TiO_2. This is accomplished as a result of the specially selected design, which has parabolic light reflectors, and the frequent replacement of the near-UV lamps.

(3) Windows in the reacting section free of deposited particles. This is achieved with a gas flow pattern promoting high shear in the near-window region. This prevents particles from being attached to the window's surface and eliminates irradiation absorption and back reflection by window-attached particles.

(4) Negligible adsorption of reactants on the reactor wall materials.

(5) Insignificant contribution of the thermal decomposition reactions.

As a result the following reactor model can be postulated

$$V\frac{dC_i}{dt} = r_i A \tag{1}$$

where V represents the total hold up of gas in Photo-CREC-Air (m^3), C_i is the "i" model pollutant concentration ($\mu mol/m^3$), r_i is the rate of photoconversion of the "i" model pollutant ($\mu mol/min{\cdot}cm^2$), and A is the uniformly irradiated mesh area holding an optimum loading of TiO_2 particles (cm^2).

In addition to Eq. 1, one has to advance a specific mathematical form for the rate of photoconversion. For instance, the initial photoconversion rate, valuable for calculation of quan-

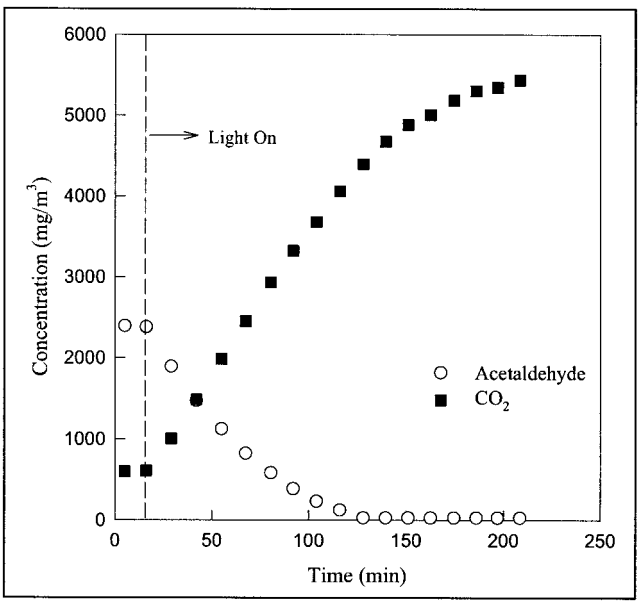

Figure 4. Photoconversion of acetaldehyde using Hombikat UV-100.

Gas phase chemical species concentration changes with reaction time.

tum efficiencies (Ibrahim and de Lasa, 2003), can be represented using a Langmuir–Hinshelwood expression as

$$r = \frac{V}{A}\frac{dC_i}{dt} = -\frac{k_i K_i C_i}{1 + K_i C_i} \tag{2}$$

where C_i represents the concentration of the "i" model pollutant and K_i and k_i represent the equilibrium adsorption and kinetic constants, respectively.

Moreover, once the photoreaction is initiated, the rate equation may involve the formation of one or more kinetically important intermediate species that can be adsorbed onto the photocatalyst surface and be detected in the gas phase. Therefore to account for this, Eq. 2 has to be modified to incorporate the gas phase intermediate concentration species, as follows

$$r = \frac{-k_i K_i C_i}{1 + K_i C_i + \sum K_j C_j} \tag{3}$$

where the term $\sum K_j C_j$ represents the combined effect of all adsorbed intermediate species, other than the model pollutant, accounted for by the summation of the product of the respective adsorption constant and the gas phase concentration.

This relatively simple model was used here to analyze the photodegradation kinetics of the various model pollutants. It was found, as discussed later, that this model provides a fairly adequate and consistent description of the chemical species concentrations in the gas phase.

Once the selection of a possible kinetics model and of a suitable reactor model (Eq. 1) was completed, a nonlinear least-square method was adopted to determine the kinetic and adsorption parameters. This was achieved by minimizing an objective function representing the sum of the differences between the model concentration estimates and the measured experimental concentrations. This nonlinear least-square fit was performed using the curve-fitting function available in Matlab (Ibrahim, 2001).

Acetone photodegradation modeling

Experimental results for the acetone photoconversion, using Degussa P25 and Hombikat UV-100, showed that acetone and carbon dioxide are the only observable gas phase species (Figure 3). Thus, on this basis and given the expected negligible carbon dioxide adsorption, the following relationships were advanced

$$r_{AC,g} = \frac{dC_{AC,g}}{dt}\frac{V}{A} = -\frac{k_{AC}K_{AC}C_{AC,g}}{1 + K_{AC}C_{AC,g}}\frac{V}{A} = -\frac{C_{AC,g}}{\theta_{1,AC} + \theta_{2,AC}C_{AC,g}}\frac{V}{A} \tag{4}$$

and

$$r_{AC,T} = (1 + K'_{AC})r_{AC,g} \tag{5}$$

where $r_{AC,g}$ is the acetone photodegradation rate assessed by the changes in the gas phase concentrations [μmol/(cm^2·min)], $r_{AC,T}$ is the total rate of acetone photodegradation [μmol/(cm^2·min)], $C_{AC,g}$ is the acetone concentration in the gas phase (μmol/m^3), A is the illuminated mesh area (cm^2), V is the total hold up of gas in Photo-CREC-Air (m^3), K_{AC} is the acetone adsorption constant (m^3/μmol), and k_{AC} is the acetone reaction rate constant (μmol/m^3·min).

The K'_{AC} or $(K_{AC}Wq_{o,AC})/V$ parameter of Eq. 5 represents the ratio of the number of micromoles of acetone adsorbed to the number of micromoles of acetone in the gas phase, where $q_{o,AC}$ is the maximum number of micromoles of acetone adsorbed per gram of catalyst (μmol/g$_{cat}$). K'_{AC} was evaluated for Degussa P25 and Hombikat UV-100 at 0.06 and 0.08, respectively (Ibrahim, 2001).

In addition, Eq. 4 can alternatively be expressed in terms of $\theta_{1,AC}$ and $\theta_{2,AC}$ parameters: $\theta_{1,AC} = 1/(k_{AC}K_{AC})$ (min) and $\theta_{2,AC} = 1/k_{AC}$ (min·m^3/μmol). This leads to a reaction rate model equation having a mathematical form displaying reduced parameter cross-correlation.

Table 1 reports the parameters obtained for three acetone concentrations, using both Degussa P25 and Hombikat UV-100, with the associated statistical indicators such as the correlation coefficient (R^2) and the sum of squared residuals (SSR).

Table 1. Summary of the Optimized Parameters for Acetone Data Modeling

Catalyst	df	R^2	SSR	$\theta_{1,AC}$ ($\times 10^{-1}$)	$\theta_{2,AC}$ ($\times 10^{3}$)
Degussa P25	115	0.99	1.06E+8	10.77 ± 0.47	4.88 ± 0.19
Hombikat UV-100	121	0.98	3.74E+8	4.06 ± 0.62	7.79 ± 0.29

Results comparing the experimental points and the fitted model are reported in Figures 5a and 6a. It can be observed that the $\theta_{1,AC}$ and $\theta_{2,AC}$ parameters, adjusted with 117–123 data points, were obtained with high correlation coefficients, 0.99 and 0.98. In addition, the calculated parameters were obtained with standard deviation spans of less than ±5%.

Therefore, the proposed model appears to be adequate to follow the acetone concentration changes in the gas phase during the photoconversion experiments. The good agreement between the model and the collected data with little mismatch of carbon dioxide [Figures 5b and 6b] supports the assumption that acetone photodegradation in Photo-CREC-Air can be viewed as acetone conversion being the rate-controlling step, with little adsorption competition of the other chemical species.

The evaluated parameters also allowed quantification of $r_{AC,g}$ at the initial reaction conditions ($t = 0$), at values of 115 and 130 μmol/(m^3·min) for Hombikat UV-100 and Degussa P25, respectively. Moreover, considering the relation between $r_{AC,g}$ and $r_{AC,T}$ (Eq.5), this yields a total acetone initial reaction rate of 125 and 137 μmol/(m^3·min) for Hombikat UV-100 and Degussa P25, respectively. Thus both photocatalysts, Hombikat UV-100 and Degussa P25, displayed a close photoactivity with apparent quantum efficiencies (ϕ), as reported by Ibrahim and de Lasa (2003), in the 50–55% range.

Acetaldehyde photodegradation modeling

Acetaldehyde photodegradation can be modeled considering, as described above, carbon dioxide and acetaldehyde as the only gas phase chemical species. Thus, it is hypothesized that

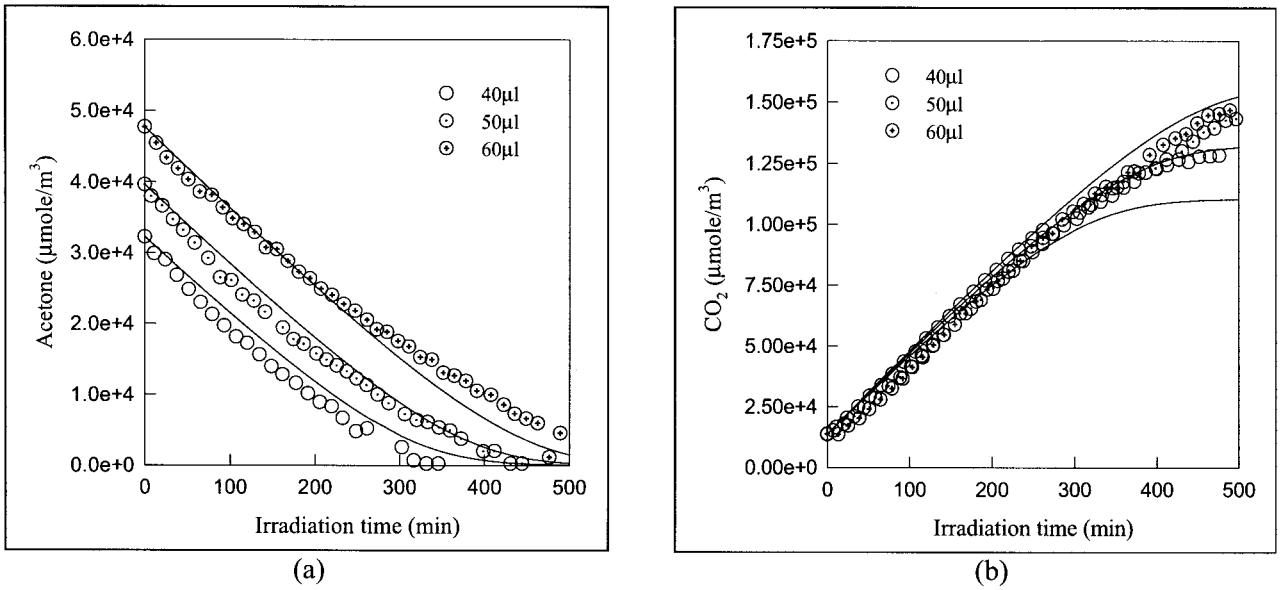

Figure 5. Changes of acetone concentrations (a) and CO_2 (b) with reaction time using Hombikat UV-100.

Full line: model predictions; circles: experimental data points.

the acetaldehyde photoconversion rates, both in Degussa P25 and in Hombikat UV-100, could be described using a Langmuir–Hinshelwood rate form as

$$r_{AA,g} = \frac{dC_{AA,g}}{dt}\frac{V}{A} = -\frac{k_{AA}K_{AA}C_{AA,g}}{1 + K_{AA}C_{AA,g}}\frac{V}{A} = -\frac{C_{AA,g}}{\theta_{1,AA} + \theta_{2,AA}C_{AA,g}}\frac{V}{A} \quad (6)$$

and

$$r_{AA,T} = (1 + K'_{AA})r_{AA,g} \quad (7)$$

where $r_{AA,g}$ is the acetaldehyde photodegradation rate assessed by gas phase concentration changes (μmol/cm^2·min), $C_{AA,g}$ is the acetaldehyde gas phase concentration (μmol/m^3), A is the illuminated mesh area (cm^2), V is the total holdup of gas in

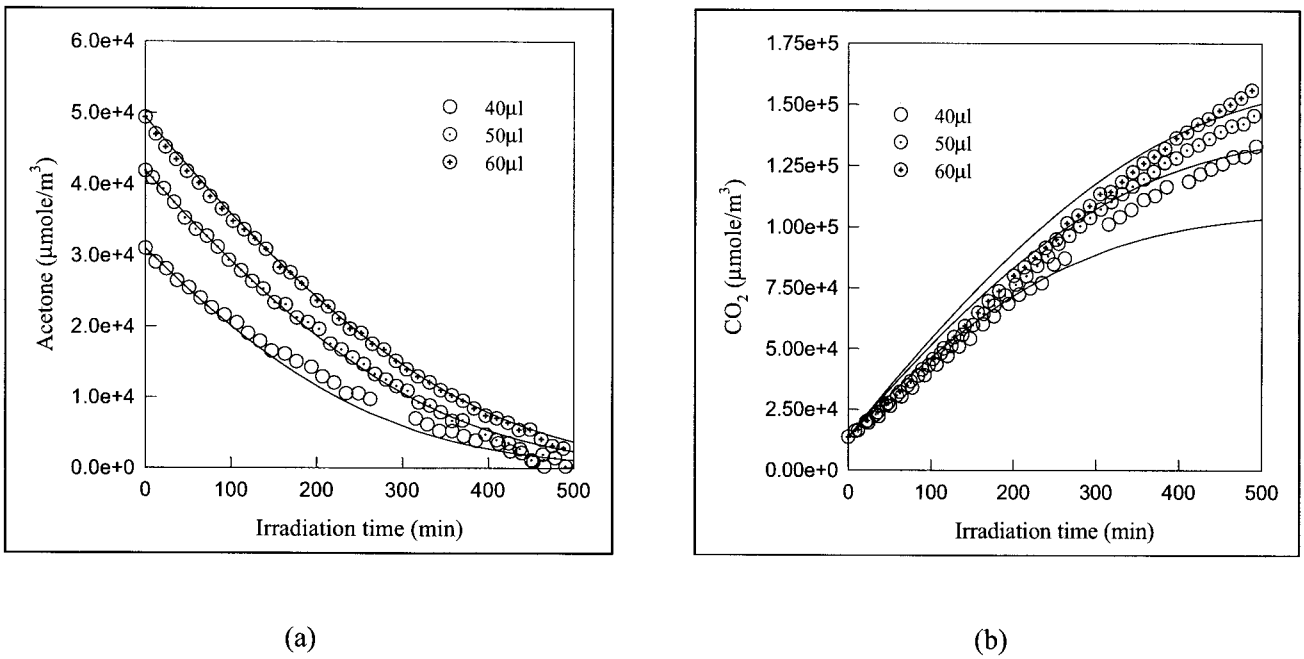

Figure 6. Changes of acetone concentrations (a) and CO_2 (b) with reaction time using Degussa P25.

Full line: model predictions; circles: experimental data points.

Table 2. Summary of the Optimized Parameters for Acetaldehyde Data Modeling

Catalyst	df	R^2	SSR	$\theta_{1,AA}$ ($\times 10^{-1}$)	$\theta_{2,AA}$ ($\times 10^{4}$)
Degussa P25	74	0.97	4.70E+08	5.10 ± 0.45	3.62 ± 1.55
Hombikat UV-100	48	0.99	1.46E+08	1.99 ± 0.218	6.87 ± 0.89

Photo-CREC-Air (m^3), K_{AA} is the acetaldehyde adsorption constant ($m^3/\mu mol$), k_{AA} is the acetone reaction rate constant ($\mu mol/m^3 \cdot min$), $r_{AA,T}$ is the total rate of acetaldehyde photodegradation [$\mu mol/(cm^2 \cdot min)$], and K'_{AA} is the ratio of the number of moles of acetaldehyde adsorbed to the number of moles of acetaldehyde in the gas phase or $(K_{AA}Wq_{o,AA})/V$. The K'_{AA} parameter of Eq. 7 was evaluated for Degussa P25 and Hombikat UV-100 at values of 0.07 and 0.13, respectively (Ibrahim, 2001).

Here again an alternate rate equation (Eq. 6) can be considered in terms of $\theta_{1,AA}$ and $\theta_{2,AA}$ parameters: $\theta_{1,AA} = 1/(k_{AA}K_{AA})$ (min) and $\theta_{2,AA} = 1/k_{AA}$ ($min \cdot m^3/\mu mol$). Regressed parameters were obtained minimizing the $\sum_{i=1}^{i=n} (C_{AA,exp,i} - C_{AA,model,i})^2$ objective function using a least-square method. The resulting parameters are reported in Table 2 with constants $\theta_{1,AA}$ and $\theta_{2,AA}$ obtained with low standard deviation and high correlation coefficients.

It can be observed that Eq. 6, with the parameters reported in Table 2, provides good estimates of the experimental data [Figures 7a and 8a], with Hombikat UV-100 data giving a somewhat better fit than that of the Degussa P25 data. On this basis, intrinsic rate constants of 2762 and 1455 $\mu mol/(m^3 \cdot min)$ were assessed for Degussa P25 and Hombikat UV-100, respectively.

The evaluated parameters also allowed quantifying the total initial reaction rate conditions using Eq. 7. This resulted in a total acetaldehyde initial reaction rate of 1073 and 833 $\mu mol/(m^3 \cdot min)$ for Hombikat UV-100 and Degussa P25, respectively. Therefore, under these conditions, Hombikat UV-100 showed a better photocatalytic activity toward acetaldehyde than did Degussa P25. Furthermore, with the initial reaction rates, the calculated apparent quantum efficiencies are in the 340–450% range (Ibrahim and de Lasa, 2003).

When the fitted parameters were used to calculate the carbon dioxide formation it was observed that the proposed model consistently predicts a faster carbon dioxide formation rate than that observed experimentally [Figures 7b and 8b]. It is only toward the end of the experiments where the cumulative CO_2 measured becomes higher than the model predictions. This phenomenon, not noticed in the case of acetone photodegradation, suggests some failure of the kinetic model assumptions. One possible explanation is the existence of strongly adsorbed and unaccounted intermediate species, presumably acetic acid, that photodegrades at a lower rate than that of acetaldehyde. In this respect, acetic acid could eventually be incorporated into the photoconversion network without, however, being present in the gas phase at detectable levels. This finding is in agreement with the results of Ohko et al. (1998), who reported that the amount of measured carbon dioxide was less than that expected from acetaldehyde photoconversion. In the study by Ohko et al. (1998), catalyst extracts revealed the presence of acetic acid, in nonnegligible amounts, and this helped to close their carbon balance.

Nimlos et al. (1996) provided additional support to a mechanism involving acetic acid and even formaldehyde. In the study by Nimlos et al. (1996), the acetic acid appeared as a detectable gas phase species, with acetic acid having an assigned adsorption constant 14 times that of acetaldehyde.

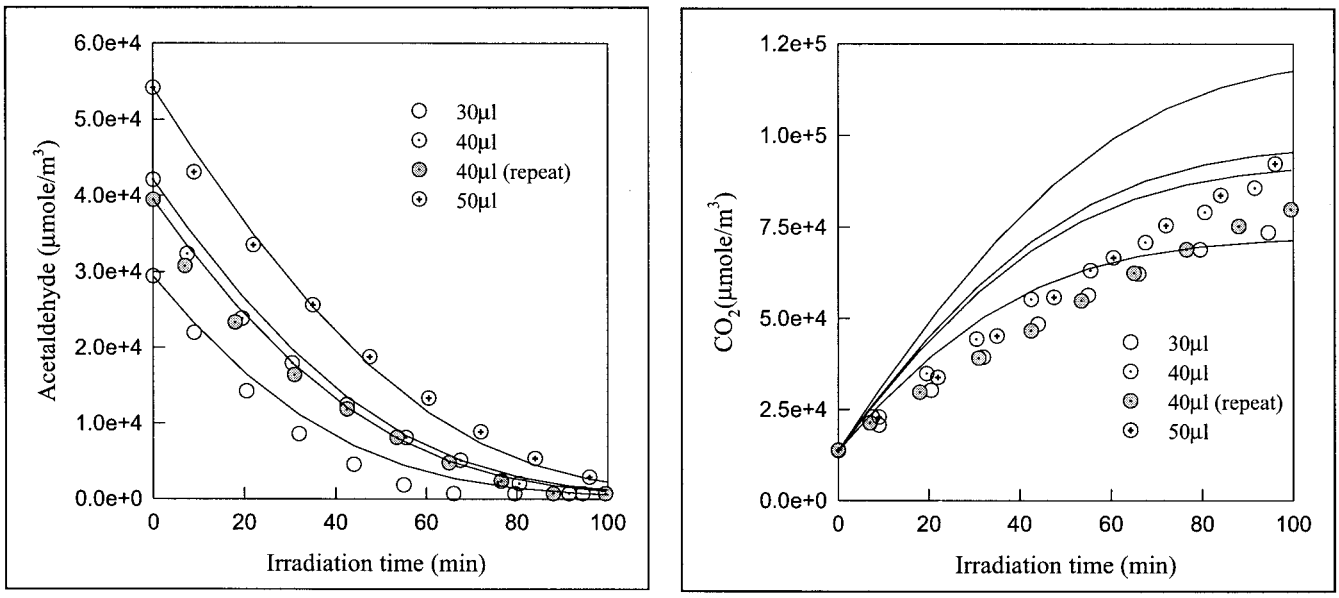

(a) (b)

Figure 7. Changes of acetaldehyde (a) and CO_2 (b) concentrations with reaction time using Hombikat UV-100.

Full line: model predictions; circles: experimental data points.

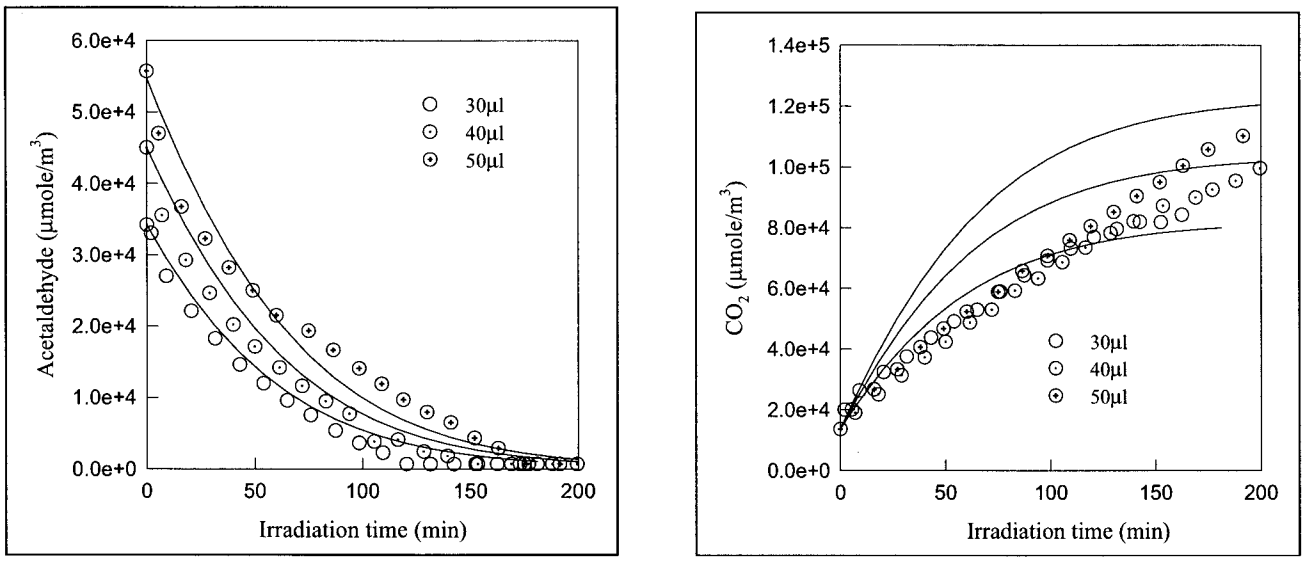

Figure 8. Changes of acetaldehyde (a) and CO_2 (b) concentrations with reaction time using Degussa P25.

Full line: model predictions; circles: experimental data points.

Consequently, the results of the present study strongly suggest that, although Eqs. 6 and 7 are satisfactory for modeling the conversion of acetaldehyde, a more sophisticated model is required for accurate carbon dioxide predictions.

Isopropanol photodegradation modeling

Isopropanol is a model compound that can be mineralized following a path that involves acetone as an observable gas phase intermediate species.

With respect to $r_{IP,g}$, it is also postulated that isopropanol photodegradation can be approximated using a Langmuir–Hinshelwood competitive model with both isopropanol and acetone competing for the same sites

$$r_{IP,g} = \frac{dC_{IP,g}}{dt}\frac{V}{A} = -\frac{k_{1,IP}K_{IP}C_{IP,g}}{1 + K_{IP}C_{IP,g} + K_{AC}C_{AC,g}}\frac{V}{A} \tag{8}$$

where $r_{IP,g}$ is the rate of isopropanol degradation as assessed by changes in the gas phase concentrations [μmol/(cm^2·min)], $C_{IP,g}$ is the concentration of isopropanol in the gas phase (μmol/m^3), $C_{AC,g}$ is the acetone gas phase concentration (μmol/m^3), A is the illuminated mesh area (cm^2), V is the total hold up of gas in Photo-CREC-Air (m^3), $k_{1,IP}$ is the reaction rate constant of the first reaction (isopropanol $\rightarrow$ acetone) (μmol/m^3·min), K_{IP} is the isopropanol adsorption constant (m^3/μmol), and K_{AC} is the acetone adsorption constant (m^3/μmol).

Equation 8 can be expressed in terms of an alternate equation as follows

$$r_{IP,g} = -\frac{C_{IP,g}}{\theta_{1,IP} + \theta_{2,IP}C_{IP,g} + \theta_{3,IP}C_{AC,g}}\frac{V}{A} \tag{9}$$

The rate of acetone photoconversion, in the context of the isopropanol degradation, can be approximated using the following relationship

$$r_{AC,g} = \frac{dC_{AC,g}}{dt}\frac{V}{A} = -\frac{k_{2,IP}K_{AC}C_{AC,g}}{1 + K_{IP}C_{IP,g} + K_{AC}C_{AC,g}}\frac{V}{A} \tag{10}$$

where $k_{2,IP}$ is the reaction rate constant of the second reaction (acetone $\rightarrow$ CO_2 + H_2O) in μmol/m^3·min.

Similarly Eq. 10 can also be expressed as

$$r_{AC,g} = -\frac{C_{AC,g}}{\theta_{4,IP} + \theta_{5,IP}C_{IP,g} + \theta_{6,IP}C_{AC,g}}\frac{V}{A} \tag{11}$$

Thus, in the Photo-CREC-Air unit, modeling the photoconversion of isopropanol involves the simultaneous solution of the following set of differential equations with $\theta_{1,IP}$, $\theta_{2,IP}$, $\theta_{3,IP}$, $\theta_{4,IP}$, $\theta_{5,IP}$, and $\theta_{6,IP}$ parameters

$$\frac{dC_{IP,g}}{dt} = -\frac{C_{IP,g}}{\theta_{1,IP} + \theta_{2,IP}C_{IP,g} + \theta_{3,IP}C_{AC,g}} \tag{12}$$

$$\frac{dC_{AC,g}}{dt} = \frac{C_{IP,g}}{\theta_{1,IP} + \theta_{2,IP}C_{IP,g} + \theta_{3,IP}C_{AC,g}}\zeta - \frac{C_{AC,g}}{\theta_{4,IP} + \theta_{5,IP}C_{IP,g} + \theta_{6,IP}C_{AC,g}} \tag{13}$$

$$\frac{dC_{CO_2}}{dt} = 3\frac{C_{AC,g}}{\theta_{4,IP} + \theta_{5,IP}C_{IP,g} + \theta_{6,IP}C_{AC,g}} \tag{14}$$

and

Table 3. Summary of the Parameters Involved in the Isopropanol Modeling

Parameter	Selected
$\theta_{1,IP}$	No
$\theta_{2,IP}$	Yes
$\theta_{3,IP}$	No
$\theta_{4,IP}$	Yes
$\theta_{5,IP}$	Yes
$\theta_{6,IP}$	Yes

$$\frac{dC_{IP,T}}{dt} = (1 + K'_{IP})\frac{dC_{IP,g}}{dt} \quad \text{and} \quad \frac{dC_{AC,T}}{dt} = (1 + K'_{AC})\frac{dC_{AC,T}}{dt} \tag{15}$$

with $\zeta = 1 + K'_{IP}/(1 + K'_{AC})$, as proposed by Ibrahim (2001).

These equations with $\zeta = 1.3$ for Degussa P25 and $\zeta = 1.15$ for Hombikat UV-100 (Ibrahim, 2001) were solved simultaneously using Matlab. Regression of parameters were obtained minimizing the following objective function

$$\sum (C_{IP,exp,i} - C_{IP,model,i})^2 + (C_{AC,exp,i} - C_{AC,model,i})^2 \tag{16}$$

Regarding the proposed model, it was observed that isopropanol showed an almost zero-order reaction, and probably first-order, at very low concentrations. Thus, to be consistent with the experimental data this means that parameters $\theta_{1,IP}$ and $\theta_{3,IP}$ are not numerically significant and can be deleted from the analysis (see Table 3).

For isopropanol photodegradation on Degussa P25, a reduced four-parameter model involving $\theta_{2,IP}$, $\theta_{4,IP}$, $\theta_{5,IP}$, and $\theta_{6,IP}$ was reexamined. Fitting of this model was performed individually for each concentration as well as for all concentrations together. Parameters obtained for this fitting are summarized in Table 4. One can notice that the optimized parameter ($\theta_{5,IP}$) was negative for most cases, which raised questions about the adequacy of including the $\theta_{5,IP}$ parameter and this suggests that the four-parameter model represents an overparameterized model and that a reduced three-parameter model, with $\theta_{2,IP}$, $\theta_{4,IP}$, and $\theta_{6,IP}$, should be considered.

Using the above-described three-parameter model, positive parameters were obtained for all the runs (Table 5). Once the fitting was completed, the parameters were used to generate the isopropanol, acetone, and carbon dioxide curves to test the model adequacy. Regarding isopropanol and acetone concentrations, very good fittings were obtained for Degussa P25 (Figure 9 and Table 5) with a less-reliable fitting for Hombikat UV-100 (Table 6).

It was also observed that the proposed model has the intrinsic difficulty that it cannot predict further increases in carbon dioxide once the acetone disappears from the gas phase and, as a result, the model tends to underpredict CO_2 concentrations toward the end of the run. This fact also points toward the existence of unaccounted intermediates, other than acetone, adsorbed onto the catalyst surface or at levels below the detectable limits in the gas phase.

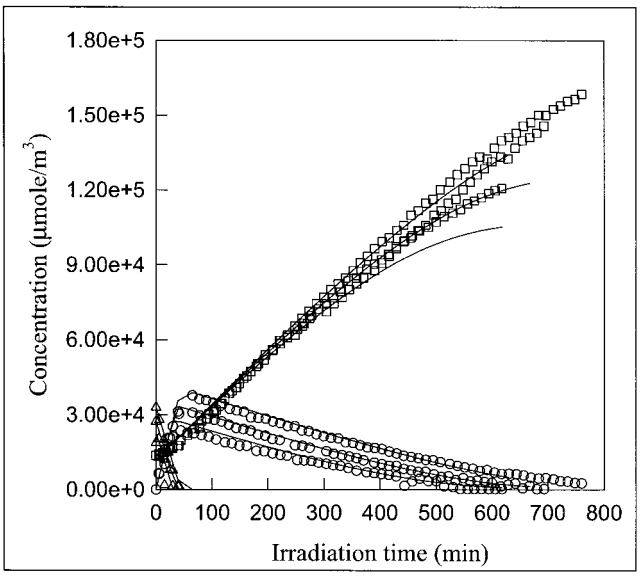

Figure 9. Changes of concentrations with reaction time for isopropanol photodegradation using Degussa P25.

Data collected for injection concentrations of 40 mL, 50 mL, and 60 μL.

Another interesting matter relates to the comparison of $\theta_{4,IP}$ and $\theta_{6,IP}$ parameter values (Tables 5 and 6) with the $\theta_{1,AC}$ and $\theta_{2,AC}$ values, as reported in Table 1. It can be observed that the reported constants are very close for Hombikat 100 and in the same order of magnitude for Degussa P25. This is encouraging given these parameters, all of which associated with acetone photoconversion were determined under quite different reaction conditions: in one case acetone was the reactant, whereas in another case it was an intermediate species of isopropanol photoconversion.

Furthermore, using the obtained parameters initial photoconversion rates for isopropanol were calculated, thus allowing estimation of apparent quantum efficiencies in the 166–420% range (Ibrahim and de Lasa, 2003).

It must be pointed out that the reported apparent quantum efficiencies represent conservative estimates, given that not all polychromatic photons reaching the TiO_2 mesh are absorbed, with a fraction of them being back reflected or forward scattered. Thus, actual quantum efficiencies could only be higher

Table 4. Optimized Parameters for the Isopropanol Photodegradation Data Using Degussa P25 and the Four-Parameter Model

Concentration (μL)	df	R^2	SSR	$(1/\theta_{2,IP})$ $(\times 10^{-2})$ (μmol/min · m^3)	$\theta_{4,IP}$ $(\times 10^{-1})$ (min)	$\theta_{5,IP}$ $(\times 10^{2})$ (min · m^3/μmol)	$\theta_{6,IP}$ $(\times 10^{3})$ (min · m^3/μmol)
40	78	0.961	2.23E+08	4.89 ± 0.19E−03	0.72 ± 0.60E−3	−4.4 ± 0.13E−03	19.8 ± 0.00
50	98	0.995	1.95E+08	7.66 ± 0.23	5.10 ± 0.37	0.39 ± 0.02	12.7 ± 0.02
60	116	0.987	4.53E+08	6.37 ± 0.17	3.27 ± 1.05	−3.2 ± 0.04	13.5 ± 0.04
All	296	0.987	6.34E+08	7.54 ± 0.13	10.9 ± 0.21	−0.12 ± 0.0007	10.5 ± 0.00

Table 5. Optimized Parameters for the Isopropanol Photodegradation Data Using Degussa P25 and the Three-Parameter Model

Concentration (μL)	df	R^2	SSR	$(1/\theta_{2,IP})$ $(\times 10^{-2})$ (μmol/min · m^3)	$\theta_{4,IP}$ $(\times 10^{-1})$ (min)	$\theta_{6,IP}$ $(\times 10^{3})$ (min · m^3/μmol)
40	79	0.974	2.03E+08	8.54 ± 0.60	5.48 ± 0.0003	14.3 ± 0.00
50	99	0.993	2.58E+08	7.93 ± 0.29	0.61 ± 0.07	15.7 ± 0.02
60	117	0.972	6.96E+08	5.69 ± 0.26	1.08 ± 0.08	15.1 ± 0.02
All	297	0.987	7.35E+08	7.44 ± 0.13	7.20 ± 0.14	12.2 ± 0.01

than the already high and encouraging apparent quantum efficiencies observed in the Photo-CREC-Air unit.

These apparent quantum efficiencies, well in excess of 100%, can be justified on the basis of the potential role assigned in the photoconversion of oxygenates to a free-radical chain mechanism involving a peroxoradical (Ohko et al., 1998).

Conclusions

On the basis of the kinetic modeling developed in the present study the following can be concluded:

(1) A Langmuir–Hinshelwood rate of reaction, involving a one-site, one-model pollutant mechanism, is adequate to describe the photodegradation of acetone on both Degussa P25 and Hombikat UV-100. However, this rate equation appears to be less appropriate for predicting carbon dioxide formation from acetaldehyde and isopropanol.

(2) These kinetic models and the related parameters are established, with the related statistical indicators, using a nonlinear least-square regression analysis.

(3) The calculated parameters allowed quantifying the performance difference between two photocatalysts and the assessment of the high apparent quantum efficiencies for acetone, acetaldehyde, and isopropanol. Apparent quantum efficiencies for acetaldehyde and isopropanol were found to be well in excess of 100%.

Acknowledgments

The authors gratefully acknowledge the Natural Science and Engineering Research Council of Canada and The University of Western Ontario Research Office.

Notation

A = uniformly irradiated mesh area holding an optimum amount of TiO_2 (cm^2)
$C_{i,g}$ = "i" pollutant concentration in the gas phase (μmol/m^3)
k_i = reaction rate constant for model pollutant "i" (μmol/m^3·min)
$k_{1,IP}$ = reaction rate constant of the first reaction (IP → acetone) (μmol/m^3·min)
$k_{2,IP}$ = reaction rate constant of the second reaction (acetone → CO_2 + H_2O) (μmol/m^3·min)
K_i = "i" chemical species adsorption constant (m^3/μmol)
K'_i = $(K_i W q_{o,i})/V$ or ratio of the number of moles of the "i" species adsorbed over the number of moles of "i" species in the gas phase
$q_{o,i}$ = maximum number of micromoles of "i" species adsorbed per gram of catalyst (μmol/g$_{cat}$)
$r_{i,g}$ = "i" species photodegradation rate calculated with gas phase concentration changes (μmol/cm^2·min)
$r_{i,T}$ = total rate of "i" species photodegradation [μmol/(cm^2·min)]
V = total hold up of gas in Photo-CREC-Air (m^3)

Subscripts

AA = acetaldehyde
AC = acetone
exp = experimental
IP = isopropanol
model = model

Greek letters

ϕ = apparent quantum efficiency (number of photoconverted model pollutant molecules/number of polychromatic photons reaching the glass mesh)
$\theta_{1,AA} = 1/(k_{AA}K_{AA})$ (min)
$\theta_{2,AA} = 1/k_{AA}$ (min·m^3/μmol)
$\theta_{1,AC} = 1/(k_{AC}K_{AC})$ (min)
$\theta_{2,AC} = 1/k_{AC}$ (min·m^3/μmol)
$\theta_{1,IP} = 1/(k_{1,IP}K_{IP})$ (min)
$\theta_{2,IP} = 1/k_{1,IP}$ (min·m^3/μmol)
$\theta_{3,IP} = K_{AC}/(k_{1,IP}K_{IP})$ (min)
$\theta_{4,IP} = 1/(k_{2,IP}K_{AC})$ (min)
$\theta_{5,IP} = K_{IP}/(k_{2,IP}K_{AC})$ (min·m^3/μmol)
$\theta_{6,IP} = 1/k_{2,IP}$ (min·m^3/μmol)
$\zeta = 1 + K'_{IP}/(1 + K'_{AC})$

Literature Cited

Cabrera, M., O. Alfano, and A. Cassano, "Novel Reactor for Photocatalytic Kinetic Studies," *Ind. Eng. Chem. Res.*, **33**, 3031 (1994).

Cassano, A., C. Martin, R. Brandi, and O. Alfano, "Photoreactor Analysis and Design: Fundamentals and Applications," *Ind. Eng. Chem. Res.*, **34**, 2155 (1995).

Cunningham, J., and B. Hodnett, "Kinetic Studies of Secondary Alcohol Photo-Oxidation on ZnO and TiO_2 at 348K Studied by Gas Chromatograph Analysis," *J. Chem Soc. Faraday Trans. 1*, **77**, 2777 (1981).

Table 6. Optimized Parameters for the Isopropanol Photodegradation Data Using Hombikat UV-100 and the Four-Parameter Model

Concentration (μL)	df	R^2	SSR	$(1/\theta_{2,IP})$ $(\times 10^{-2})$ (μmol/min · m^3)	$\theta_{4,IP}$ $(\times 10^{-1})$ (min)	$\theta_{5,IP}$ $(\times 10^{2})$ (min · m^3/μmol)	$\theta_{6,IP}$ $(\times 10^{3})$ (min · m^3/μmol)
40	44	0.9661	1.2E+08	3.34 ± 0.03	0.407 ± 1.59	24.9 ± 45.9	8.55 ± 1.28
50	72	0.9849	1.91E+08	3.24 ± 0.06	5.56 ± 0.785	4.31 ± 0.06	7.09 ± 0.28
60	98	0.986	3.2E+08	3.15 ± 0.05	3.825 ± 0.914	2.73 ± 0.00	9.13 ± 0.43
All	302	0.977	1.01E+09	3.19 ± 0.00	3.83 ± 0.00	6.01 ± 0.0	8.16 ± 0.00

Falconer, J., and K. Magrini-Bair, "Photocatalytic and Thermal Oxidation of Acetaldehydeon Pt/TiO_2," *J. Catal.*, **179**, 171 (1998).
Fox, M., "Photocatalytic Oxidation of Organic Substances," in *Photocatalysis and Environment: Trends and Applications*, M. Schiavello, ed., Kluwer Academic, Dordrecht, The Netherlands, pp. 445–467 (1988).
Ibrahim, H., "Photocatalytic Reactor for the Degradation of Airborne Pollutants. Photo-conversion Efficiency and Kinetic Modeling," PhD Dissertation, The University of Western Ontario, Canada (2001).
Ibrahim, H., and H. de Lasa, "Photo-catalytic Conversion of Air Borne Pollutants. Effect of Catalyst Type and Loading in Novel Photo-CREC-Air Unit," *Appl. Catal.*, **38**, 201 (2002).
Ibrahim, H., and H. de Lasa, "Photo-Catalytic Degradation of Air Borne Pollutants. Apparent Quantum Efficiencies in a Novel Photo-CREC-Air Reactor," *Chem. Eng. Sci.*, **58**, 943 (2003).
Jacoby, W., D. Black, D. Fennel, J. Boutlet, L. Vargo, M. George, and S. Dolberg, "Heterogenous Photocatalysis for control of Volatle Organic Compounds in Indoor Air," *J. Air Waste Management Assoc.*, **46**, 691 (1996).
Luo, Y., and D. Ollis, "Heterogeneous Photocatalytic Oxidation of Trichloroethylene and Toluene Mixtures in Air: Kinetic Promotion and Inhibition, Time-Dependent Catalyst Activity," *J. Catal.*, **163**, 1 (1996).
Miller, R., and R. Fox, "Treatment of Organic Contaminants in Air by Photocatalytic Oxidation: A Commercialization Perspective," in *Photocatalytic Purification and Treatment of Water and Air: Proceedings of the 1st International Conference on TiO_2*, D. Ollis and H. Al-Ekabi, eds., Elsevier, New York, 573 (1993).
Nimlos, M., E. Wolfrum, M., Brewer, J. Fennell, and G. Bintner, "Gas Phase Heterogeneous Photocatalytic Oxidation of Ethanol: Pathways and Kinetic Modeling," *Environ. Sci. Technol.*, **30**(10), 3102 (1996).
Ohko, Y., and A. Fujishima, "Kinetics Analysis of the Photocatalytic Degradation of Gas-Phase 2-Propanol Under Mass Transport-Limited Conditions with a TiO_2 Film Photocatalyst," *J. Phys. Chem. B*, **102**, 1724 (1998).
Ohko, Y., D. Tryk, K. Hashimoto, and A. Fujishima, "Autoxidation of Acetaldehyde by TiO_2 Photocatalysis Under Weak UV Illumination," *J. Phys. Chem. B*, **102**(15), 2699 (1998).
Peral, J., and D. Ollis, "Heterogeneous Photocatalytic Oxidation of Gas-Phase Organics for Air Purification: Acetone, 1-Butanol, Butyraldehyde, Formaldehyde, and *m*-Xylene Oxidation," *J. Catal.*, **136**, 554 (1992).
Raupp, G., and C. Junio, "Photocatalytic Oxidation of Oxygenated Air Toxics," *Appl. Surf. Sci.*, **72**, 321 (1993).
Shifu, C., C. Xueli, T. Yaowu, and Z. Mengyue, "Photocatalytic Degardation of Trace Gaseous Acetone and Acetaldehyde Using TiO_2 Supported on Fiberglass Cloth," *J. Chem. Technol. Biotechnol.*, **73**, 264 (1998).
Suri, R., J. Liu, D. Hand, J. Crittenden, D. Perram, and M. Mullims, "Heterogeneous Photocatalytic Oxidation of Hazardous Organic Contaminants in Water," *Water Environ. Res.*, **65**(5), 665 (1993).
Suzuki, K., "Photocatalytic Air Purification on TiO_2 Coated Honeycomb Support," in *Photocatalytic Purification and Treatment of Water and Air: Proceedings of the 1st International Conference on TiO_2*, D. Ollis and H. Al-Ekabi, eds., Elsevier, New York, pp. 412–434 (1993).
Yue, P., "Modeling, Scale up and Design of Multiphasic Photoreactors," in *Photocatalytic Purification and Treatment of Water and Air: Proceedings of the 1st International Conference on TiO_2*, D. Ollis and H. Al-Ekabi, eds., Elsevier, New York, 495 (1993).

Manuscript received Nov. 14, 2002, and revision received Aug. 19, 2003.